


Article

Thermal Decomposition Characteristics of PEO/LiBF₄/LAGP Composite Electrolytes

Jacob Denney and Hong Huang * 

Department of Mechanical and Materials Engineering, Wright State University, Dayton, OH 45435, USA; denney.3@wright.edu

* Correspondence: hong.huang@wright.edu

Abstract: Lithium-based batteries with improved safety performance are highly desired. At present, most safety hazard is the consequence of the ignition and flammability of organic liquid electrolytes. Dry ceramic-polymer composite electrolytes are attractive for their merits of non-flammability, reduced gas release, and thermal stability, in addition to their mechanical strength and flexibility. We recently fabricated free-standing solid composite electrolytes made up of polyethylene oxide (PEO), LiBF₄ salt, and Li_{1+x}Al_xGe_{2-x}(PO₄)₃ (LAGP). This study is focused on analyzing the impacts of LAGP on the thermal decomposition characteristics in the series of PEO/LiBF₄/LAGP composite membranes. It is found that the appropriate amount of LAGP can (1) significantly reduce the organic solvent trapped in the polymer network and (2) increase the peak temperature corresponding to the thermal degradation of the PEO/LiBF₄ complex. In the presence of LAGP, although the peak temperature related to the degradation of free PEO is reduced, the portion of free PEO, as well as its decomposition rate, is effectively reduced, resulting in slower gas release.

Keywords: lithium; LAGP; electrolyte; composite; thermal decomposition



Citation: Denney, J.; Huang, H.

Thermal Decomposition

Characteristics of PEO/LiBF₄/LAGP

Composite Electrolytes. *J. Compos.*

Sci. **2022**, *6*, 117. [https://doi.org/](https://doi.org/10.3390/jcs6040117)

10.3390/jcs6040117

Academic Editor: Stelios

K. Georgantzinou

Received: 20 March 2022

Accepted: 11 April 2022

Published: 14 April 2022

Publisher's Note: MDPI stays neutral with regard to jurisdictional claims in published maps and institutional affiliations.



Copyright: © 2022 by the authors. Licensee MDPI, Basel, Switzerland. This article is an open access article distributed under the terms and conditions of the Creative Commons Attribution (CC BY) license (<https://creativecommons.org/licenses/by/4.0/>).

1. Introduction

Lithium-ion batteries (LIBs), because of their high energy density and good discharge/charge cycle life, have evolved and dominated in markets from powering electronic devices and electric vehicles to energy storage in renewable grid systems. In these broad applications, occasional firing or explosive accidents resulting from LIBs have raised serious concerns. At present, battery researchers and manufacturers are dedicating to develop lithium-based batteries with improved safety performance, in addition to enhancing their power specs [1–7]. External protections, with the help of electronic accessories, like thermal fuse, pressure vents, and PTC element, have been integrated in LIB batteries to mitigate thermal runaway. However, internal protection based on the choice of safe materials is believed to be the “ultimate” solution to the safety issue. Recently, many key battery components have been developed towards minimizing thermal runaway, including surface-modified electrodes, non-flammable electrolytes, multifunctional separators, overcharging or flame-retardant additives, and thermally switchable current collectors.

Solid electrolytes, referring to ion-conducting ceramics or dry polymers, as well as polymer–ceramic composites, have many merits and are known for non-volatility, non-flammability, and high thermal decomposition temperatures, etc., to address the safety issues [8,9]. Composite polymer electrolytes (CPEs), which combine characteristics of polymer and ceramic electrolytes, with potential to overcome the drawbacks of each kind, are becoming more attractive [10–13]. For instance, the unique mechanical properties of CPEs provide enough strength to resist lithium dendrite penetration and meantime flexibility to ensure good interface contact. All-solid-state LIBs made up of CPEs are becoming more attractive and are recognized as a key technology for next-generation energy-storage systems.

Research on the thermal stability and safety of LIBs made up of dry CPEs is still in the infancy stage [14]. Extensive studies on CPEs had emphasized on increasing ionic conductivity, improving mechanical flexibility, and enhancing interfacial stability [15–23]. In the published reports, most thermal characteristics of CPEs presented are limited to temperatures below 100 °C, within which the glass transition temperature (T_g) and crystallization temperature (T_c) are known to be critical to ionic conductivities. In some papers, thermalgravimetric decomposition profiles up to 500 °C were presented, while in-depth analyses on the decomposition behaviors of CPEs are lack of discussion. Among sparse reports on thermal stabilities of PEO (polyethylene oxide)-based electrolytes, inconsistencies or controversial conclusions are noted. Xia and Angulakshimi [24,25] observed that the addition of LiTFSI to PEO increased thermal decomposition temperature (T_{dec}) of PEO from 200 °C to 300 °C. However, Joost [26] found that T_{dec} of PEO was lowered in PEO/LiTFSI and that the decomposition has multiple stages. Similarly to CPE systems, Cheng [27] found that adding 30% LLZO increased the T_{dec} of PEO, while Piana [28] observed an opposite trend in the PEO/LAGP-based electrolytes.

Among various CPE formulations, active ceramic fillers with high ionic conductivities are favorable, especially when a high content of ceramic fillers is required. $\text{Li}_{1+x}\text{Al}_x\text{Ge}_{2-x}(\text{PO}_4)_3$ (LAGP) is known for its high room-temperature ionic conductivity (10^{-3} – 10^{-4} S/cm) and good stability with moisture. Furthermore, it is risk-free of thermal runaway and subsequent fires and allows high-temperature operation [29–32]. Researchers have studied the electrochemical characteristics of PEO/LiTFSI/LAGP systems and demonstrated their satisfactory cycling and rate performances in lithium-ion, as well as lithium batteries [33–36]. In our previous publications, we have reported the method of fabricating free-standing lithiated PEO with LAGP solid composite electrolytes and investigated the impacts of lithium salt and LAGP loading on electrical and mechanical properties [37,38]. To our knowledge, there is sparse in-depth research on thermal stability and safety matters in the PEO/Li-salt/LAGP electrolyte systems, especially with the composition of high LAGP loadings. This study is focused on understanding the impact of LAGP ceramic loadings on thermal decomposition characteristics of PEO and LiBF_4 in the PEO/ LiBF_4 /LAGP composite systems. LiBF_4 salt was selected in consideration of its favorable conducting merits in liquid electrolytes and its thermal properties fundamentally distinguished from LiTFSI. We performed in-depth quantitative analyses based on the thermogravimetric results, which will be presented in this paper.

2. Materials and Experimental

A series of free-standing membranes from pure PEO, PEO/ LiBF_4 , to lithiated PEO with different amounts of $\text{Li}_{1.4}\text{Al}_{0.4}\text{Ge}_{1.6}(\text{PO}_4)_3$ (LAGP) were fabricated and analyzed in this study. PEO at a molecular weight of 400,000, anhydrous LiBF_4 , and anhydrous acetonitrile (AN) are all purchased from Sigma-Aldrich without further treatment. LAGP powders were synthesized via a two-step solid reaction method. The mixture of precursors was firstly heated at 600 °C for 6 h in air at a rate of 1 °C/min. The resultant powders were then subjected to milling in a high-energy shaker mill (SPEX Sample Prep 8000M Mill, Metuchen, NJ, USA) for 3 h before firing at 900 °C at a rate of 2 °C/min for 24 h in air. The as-synthesized LAGP powders were further milled for 24 h until the average particle size was in the sub-micron range.

Acetonitrile is the solvent used to dissolve PEO and LiBF_4 . LAGP, LiBF_4 , and PEO with predetermined compositions were mixed in AN at 50 °C in a dry room with a controlled moisture level. Afterwards, the viscous solution was transferred into a glove box (with moisture less than 5 ppm). Casting and drying were executed in the glove box at a pressure of 1 kPa followed by a constant argon flow at room temperature for up to five days. All of the membranes were sealed and stored in the glove-box prior to usage. Detailed synthesis process, structures, morphologies, and ionic conductivities of the electrolyte membranes were reported elsewhere [37].

In all of the electrolyte membranes, the molar ratio of EO to Li is fixed at 8.0 which was reported to have highest ionic conductivity [39]. This value corresponds to the mass ratio of 3.75 between PEO and LiBF₄, i.e., $\frac{m_{PEO}}{m_{LiBF_4}} = 3.75$. The composition of LAGP relative to (PEO + LAGP), i.e., $(\frac{m_{LAGP}}{m_{PEO}+m_{LAGP}})$, increases from 20 wt% to 60 wt%.

The nomenclature of the samples, the nominal weight percentage of each component and corresponding mass ratios are listed in Table 1.

Table 1. The nomenclature of the composite electrolyte membranes and the nominal composition of each component in the samples.

Sample Name	LAGP (wt%)	PEO (wt%)	LiBF ₄ (wt%)	$\frac{m_{LAGP}}{m_{PEO}+m_{LAGP}}$	$\frac{m_{PEO}}{m_{LiBF_4}}$
PEO	0	100	0		
PEO/LiBF ₄	0	78.95	21.05		3.75
LAGP20	16.48	65.93	17.58	0.20	3.75
LAGP30	25.28	58.99	15.73	0.30	3.75
LAGP40	34.48	51.72	13.79	0.40	3.75
LAGP50	44.12	44.12	11.76	0.50	3.75
LAGP60	54.22	36.14	9.63	0.60	3.75

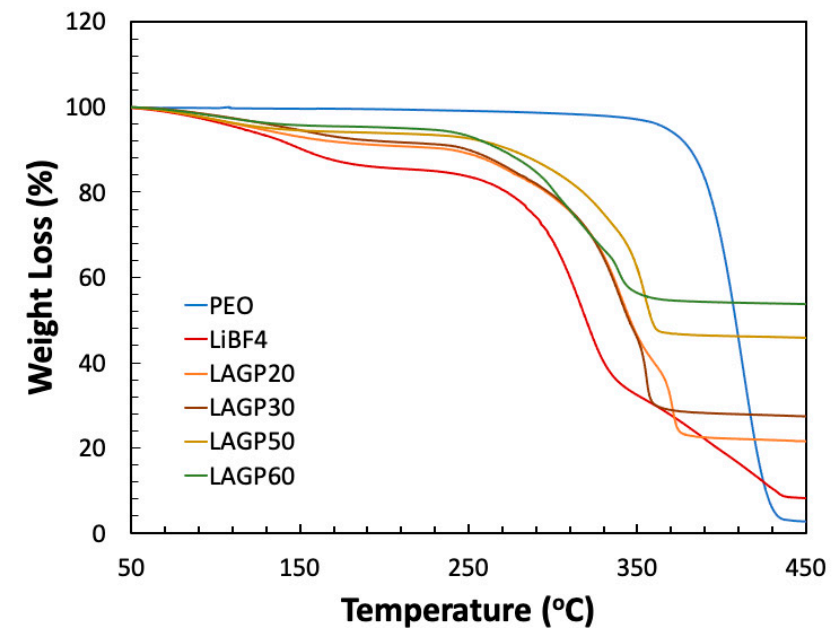
All of the samples were analyzed using the TA Instrument TGA Q5000. A few preliminary tests were performed to determine the appropriate temperature range. Excluding the LAGP portion, all other components completely decomposed below 450 °C. Hence the systematic TGA tests were set from room temperature to 450 °C. The heating rate was varied from 5 to 20 °C/min. At different heating rate, the characteristics of the TGA profile did not alter except the temperatures of weight loss uniformly shifted with the heating rate, which is common in thermal analyses. Hence, a high heating rate of 20 °C/min was selected in this study to align with the rapid thermal runaway process. The samples weighted between 15 mg and 20 mg were loaded into open platinum pans. The purge gas was nitrogen. The sample flow rate was 25 mL/min and the balance purge gas ran at a flow rate of 10 mL/min. TA Trios software was used to calculate the first derivative thermogravimetric data (DTG). The weight loss was determined from TGA profiles. The onset temperature, (T_{onset}), the peak temperature (T_p), and the max weight loss rate within each thermal event were determined from the DTG profiles.

3. Results and Discussion

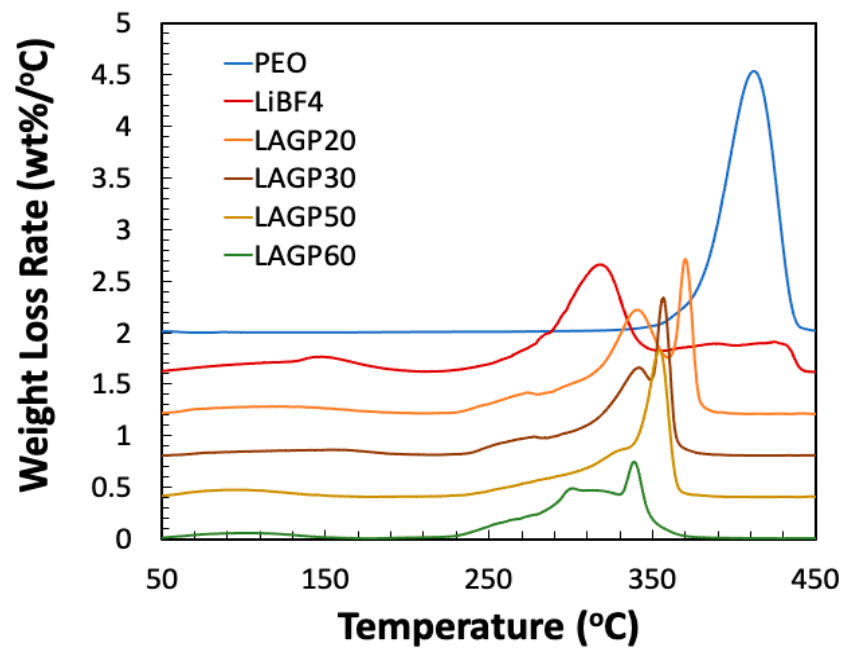
The TGA and DTG profiles of the PEO/LiBF₄/LAGP series are shown in Figure 1a,b. For better comparison and visualization, the TGA plots superimpose all together while the DTG profiles are plotted with a constant offset on the y-axis. Three distinguishable thermal events are observed from the electrolyte membranes. An initial small amount of weight loss occurs in the temperature range of 60–160 °C. Major weight loss onsets in the vicinity of 230 °C for all the electrolyte membranes independent of LAGP content. The thermal decomposition completes at 430 °C or lower. Within 230 °C and 430 °C, the electrolyte membranes exhibit two distinct thermal events with a different peak temperature and max decomposition rate. When the temperature exceeds 430 °C, the weight remains constant, showing a long plateau. The amount of weight loss, onset and peak temperatures, and the weight loss rate appear to vary with membrane compositions, which will be analyzed and discussed in the following section.

Figure 2 plots the first event weight loss (below 160 °C) as a function of LAGP amount. With increasing LAGP amount in the CPE membranes, the weight loss within this temperature range shows a reducing trend. Commercial pure LiBF₄ salt with no special treatment is known to contain traces of HF acid, which is inevitable upon exposure to moisture in production and storage. According to Lu [40], about 2.1 wt% weight loss peaked at 73 °C was observed in TGA from pure anhydrous LiBF₄, resulting from the free HF acid

removal. Based on the composition of LiBF_4 in our electrolyte membranes, the maximum HF acid amount is estimated to be less 0.4 wt%. However, seen in Figure 2, the PEO/ LiBF_4 membrane has a total weight loss of 12.8 wt% below 160 °C. In the LAGP60 membrane, the weight loss decreases to 4.5 wt% but still more than ten times the estimated HF amount. Since all our membranes were fabricated in a dry room and stored in a glove box with moisture less than 5 ppm, this weight loss cannot be related to the removal of free HF or any uptake moisture.



(a)



(b)

Figure 1. (a) TGA and (b) DTG profiles (offset by 0.4 interval for better visualization), obtained from the series of PEO/ LiBF_4 /LAGP composite electrolyte membranes. For comparison, pure PEO plots are included.

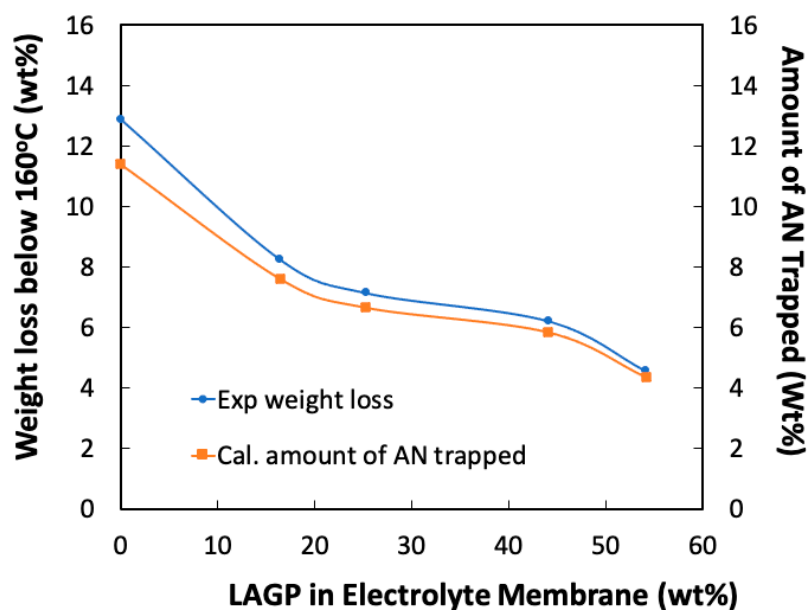


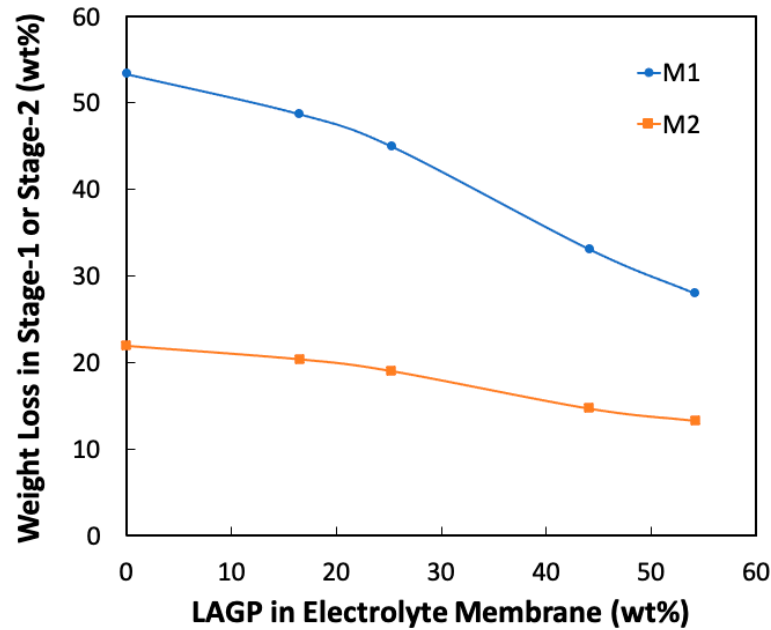
Figure 2. The experimental weight loss below 160 °C and the calculated amount of AN solvent trapped in the electrolyte membranes as a function of LAGP content.

In fabricating polymer electrolyte membranes, acetonitrile solvent was used to dissolve the PEO and LiBF_4 salt. Due to the strong interaction between LiBF_4 and acetonitrile, a certain amount of AN solvent could be trapped within the electrolyte membranes after the drying process. This phenomenon was reported previously [41,42]. The boiling point of acetonitrile is 82 °C. When it is associated with a lithium salt, the evaporation temperature will increase but can be completely evaporated under 160 °C [43]. Accordingly, we submitted that the weight loss between 60 °C and 160 °C observed in the electrolyte membranes corresponds to the amount of AN trapped. Based on the membrane composition and the weight loss, the amount of AN trapped is calculated and also plotted as a function of LAGP loading (see Figure 2). In the neat PEO membrane, there is only 0.35 wt% AN solvent trapped. By contrast, 11.4 wt% AN is trapped in the PEO/ LiBF_4 electrolyte membrane. Interestingly, the addition of ceramic LAGP appears to weaken the LiBF_4 -AN interaction, leading to the gradually reduced amount of AN in the membranes. The impact of LAGP is also reflected by the slightly decreased evaporation rate and inflection point as a function of LAGP content (see Figure 1b).

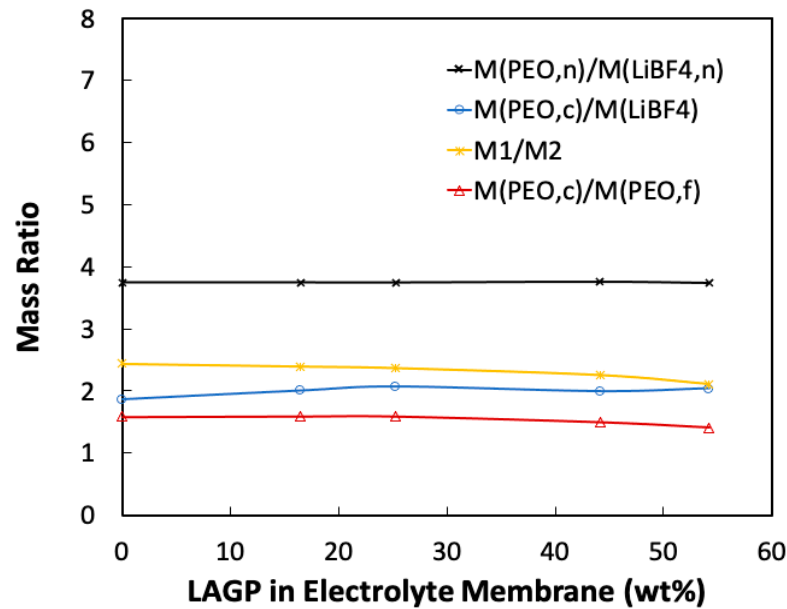
The major weight loss seen between 230 °C to 430 °C is the consequence of the thermal decomposition of LiBF_4 and PEO, as LAGP is known to be inactive to either LiBF_4 or PEO and remains thermally stable below 450 °C. Pure LiBF_4 powder or PEO membrane completes thermal decomposition in one event peaked at 277 °C and 417 °C, respectively, consistent with previous reports [40,44,45]. Seen in Figure 1, all the electrolyte membranes exhibit two distinct thermal events, with different weight-loss slopes (see Figure 1a) and two rate peaks (see Figure 1b), in this temperature range. Hereby, we refer to the two thermal events as stage-1 and stage-2 decompositions of the electrolyte membrane. The transition temperature ($T_{1 \rightarrow 2}$) from stage-1 to stage-2 is selected at the saddle point between the two weight-loss rate peaks. Stage-1 regime (230 °C to $T_{1 \rightarrow 2}$) is related with decomposition of LiBF_4 , while stage-2 regime ($T_{1 \rightarrow 2}$ to 430 °C) is the characteristic of free PEO decomposition.

Figure 3a plots the weight loss at each stage, i.e., M_1 for stage-1 and M_2 for stage-2, as a function of the LAGP content. It is interesting to see that M_1 is more than the nominal amount of Li-salt, suggesting that a portion of PEO are complexed with LiBF_4 and degraded at the lower temperature. Considering the M_1 value is the sum of all the LiBF_4 (M_{LiBF_4}) and complexed PEO portion ($M_{\text{PEO},c}$) in the electrolyte, i.e., $M_1 = M_{\text{LiBF}_4} + M_{\text{PEO},c}$, the mass ratio of $\frac{M_1 - M_{\text{LiBF}_4}}{M_{\text{LiBF}_4}}$ will reflect the mass ratio between PEO and LiBF_4 in the complex. Therefore, $\frac{M_1 - M_{\text{LiBF}_4}}{M_{\text{LiBF}_4}} = \frac{M_{\text{PEO},c}}{M_{\text{LiBF}_4}}$. On the other hand, the M_2 value corresponds to

the remanent PEO portion that are free or has much weak interaction with Li-salt. In we define $M_2 = M_{PEO,f}$, then $\frac{M_1 - M_{LiBF_4}}{M_2} = \frac{M_{PEO,c}}{M_{PEO,f}}$.



(a)



(b)

Figure 3. (a) Mass losses in stage-1 (M_1) and stage-2 (M_2) between 230 °C and 430 °C; (b) mass ratios, i.e., M_1/M_2 , calculated $M_{PEO,c}/M_{LiBF_4}$ in the complex, $M_{PEO,c}/M_{PEO,f}$, as well as nominal $M_{PEO,n}/M_{LiBF_4,n}$ in the electrolytes membranes, in correlation with LAGP content.

Figure 3b show that the series of mass ratios, i.e., $\frac{M_1}{M_2}$, $\frac{M_{PEO,c}}{M_{LiBF_4}}$, $\frac{M_{PEO,c}}{M_{PEO,f}}$, as a function of LAGP content in the membrane. For comparison, the nominal ratio between PEO and $LiBF_4$, $\frac{M_{PEO,n}}{M_{LiBF_4,n}} = 3.75$, is also included in Figure 3b. Interestingly, all the mass ratios

change insignificantly with LAGP content. From the values of $\frac{M_{PEO,c}}{M_{LiBF_4}}$, it is determined that the EO/Li⁺ molar ratio is in the range of 4.0–5.0 for all the electrolyte membranes. This observation corroborates well with the fact that PEO and lithium salt can readily form complexes with EO/Li ratio in the range of 4–6 [46,47]. The present results suggest that stable complexes of (PEO)_nLiBF₄ exist in all the PEO/LiBF₄/LAGP membranes and they are dominant in the thermal degradation within stage-1. Seen also in Figure 3b, $\frac{M_{PEO,c}}{M_{PEO,f}}$ changes insignificantly with LAGP content, indicating the portion between the complex PEO and free PEO is constant in all of the electrolyte membranes.

Figure 4 plots the peak decomposition temperatures related with the two thermal events. In the PEO/LiBF₄ membrane, the peak decomposition temperature of stage-1 ($T_{p,1}$) is at 318 °C, higher than pure LiBF₄ (277 °C), but much lower than free PEO (417 °C). The stage-2 decomposition at an almost constant rate is centered around 415 °C, characteristic of free PEO. Apparently, the “complexed” PEO appears less stable than “free” PEO, possibly catalyzed by LiBF₄. In the electrolyte membranes consisting of LAGP, $T_{p,1}$ increases to 345 °C in LAGP20, followed by a slightly decrease to 331 °C in LAGP50. $T_{p,1}$ recovers to 317 °C in LAGP60. This trend can be attributed to the impacts of excess LAGP on weakening interactions between PEO and LiBF₄. The presence of LAGP has a more significant impact on the free PEO decomposition at stage-2. The peak temperature of “free PEO” ($T_{p,2}$) is reduced to 370 °C in LAGP20 membrane and gradually recesses till to 339 °C in LAGP60 membrane. LAGP appears to accelerate the free PEO decomposition at reduced temperatures.

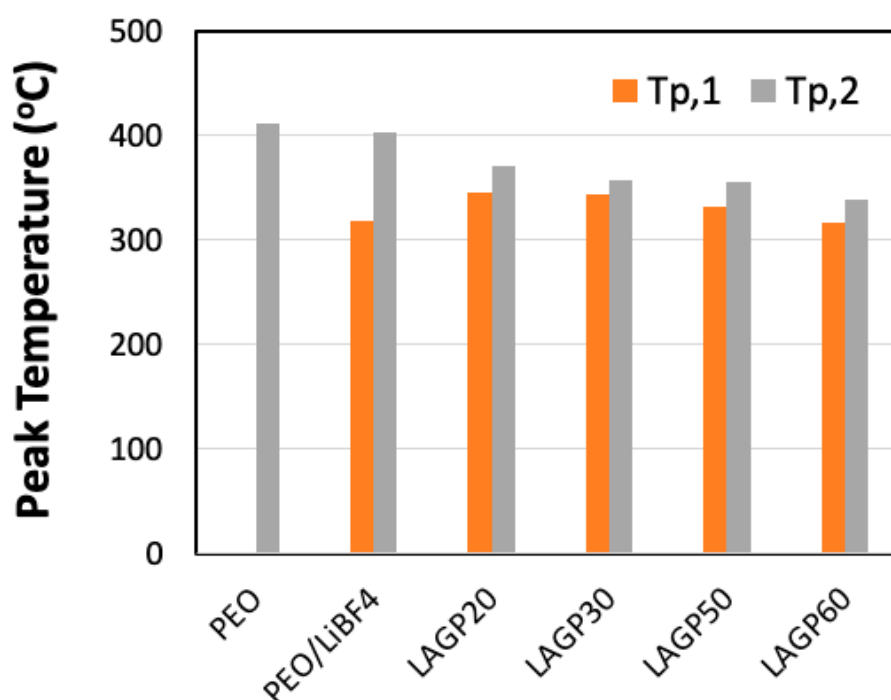


Figure 4. Two peak temperatures, $T_{p,1}$ and $T_{p,2}$, within the major decomposition occurred in all the membranes.

The 450 °C residue in all the electrolyte membranes should be made up of the nominal LAGP, LiF decomposed from LiBF₄, and PEO ashes. The actual amount of PEO ashes, calculated by subtracting the masses of LAGP and LiF from the residue, is plotted as a function of LAGP (see Figure 5). Neat PEO results in ash residue of 2.06 wt% at 450 °C. For comparison, the projected values, assuming the ash is proportional to the PEO amount, is also plotted in Figure 5. Results show that the actual PEO ash from the PEO/LiBF₄ electrolyte is only 1.02 wt%, about 60% of the projected value. The actual amount of PEO ashes continuously decreases upon increasing LAGP content and reaches almost

zero in the LAGP60 membrane. This observation supports the findings discussed in the previous session that the presence of lithium-salt and LAGP ceramics catalytically accelerate PEO decomposition.

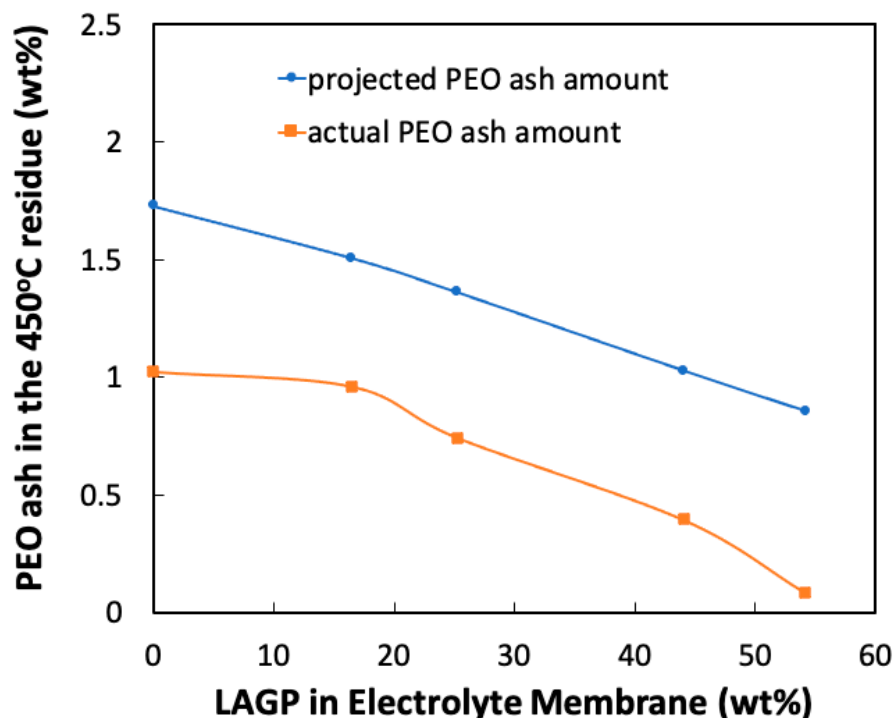


Figure 5. Projected and actual amount of PEO ashes in the 450 °C residue from all of the electrolyte membranes in relation with the nominal LAGP composition.

The impacts of LAGP on the thermal stability of the electrolyte membranes can be considered in the following aspects. Firstly, adding ceramics effectively reduces the active amount of polymer and lithium salt, and hence, the amount of gas release resulting from their decomposition [48]. This is readily observed from the TGA profiles. Seen in Figure 1a, the total released gas at 450 °C is 90 wt% for PEO/LiBF₄, 70 wt% for LAGP30, and only 30 wt% for LAGP60. Taking occurrence at 50% mass loss, the temperature increases from 320 °C for PEO/LiBF₄, to 345 °C for LAGP20 and 360 °C for LAGP50. Secondly, the major decomposition rate decreases and peak temperature increases in the presence of appropriate LAGP. Seen in Figure 1b, the maximum decomposition rate at the peak temperature is much lower in PEO/LiBF₄ compared with virgin PEO membrane. As LAGP composition increases, the maximum decomposition rate is continuously decreasing. For the stage-1 decomposition event, the peak rate is 1.0 wt% per °C occurring at 320 °C for PEO/LiBF₄, while the peak rate is reduced to 0.4 wt% per °C occurring at 336 °C for LAGP50. Thirdly, although the presence of LAGP reduces the peak decomposition temperature of the “free PEO” portion (about 40 wt% of total PEO composition), the presence of LAGP reduces the gas-release rate simultaneously. For instance, the stage-2 peak decomposition rate is 2.6 wt% per °C for the neat PEO membrane but this rate reduces to 1.3 wt% per °C for the LAGP50 electrolyte membrane. In general, a reduced decomposition rate can delay flame ignition and spread over the material [35]. We performed a flammability test on the PEO/LiBF₄/LAGP membranes. Neat PEO and PEO/LiBF₄ electrolyte membranes were easily ignited and quickly burned into ashes upon contact with flame. A significant reduction in flammability with self-extinguishing behavior was observed in the LAGP20 and LAGP30 membranes. When LAGP content is 50 wt% or greater, the composite electrolyte membranes could not be ignited even after repeated exposure and direct contact with the flame. This observation is consistent with Guo’s results from the

PvDF-HFP/LiTFSI/LAGP system [35]. The thermally stable LAGP ceramic can act as a barrier capable of reducing/preventing ignition and flammability.

4. Conclusions

This study was intended to perform in-depth quantitative analyses on the series of free-standing PEO/LiBF₄/LAGP composite electrolyte membranes based on thermogravimetric results. Major thermal decomposition begins at 230 °C and completes at 430 °C, observed in all of these electrolyte membranes. It is found that the present membrane fabrication and drying process results in 11 wt% of AN solvent trapped in the PEO/LiBF₄ electrolyte membrane. The AN in the electrolyte membrane will not only lead to potential safety concerns but also affect electrochemical performance. The presence of LAGP can effectively reduce the amount of AN trapped in the membrane when drying at room temperature. The decomposition of PEO/LiBF₄ shows a maximum rate of 1.0 wt% per °C at 320 °C, much lower than neat PEO. The reduction can be attributed to the complex formation between PEO and Li-salt. Adding and increasing the amount of LAGP ceramic particles into the PEO/LiBF₄ electrolyte system, there are several benefits towards improving the thermal stability of the electrolyte membrane. Increasing the LAGP composition in the electrolyte membrane effectively reduces the net amount of flammable PEO and LiBF₄, as well as the solvent trapped in the electrolyte membrane. As a result, the net amount of gas release from the electrolyte membrane can be significantly reduced upon thermal decomposition. With an appropriate amount of LAGP (e.g., 20–30 wt%), the peak temperature reflecting decomposition of the PEO/LiBF₄ complex can be increased by several tens of degrees Celsius. Although the decomposition of free PEO portion in the electrolytes occurs at a lower temperature in the presence of LAGP, its peak decomposition rate is reduced, which is beneficial to delay flame ignition and spread and, therefore, to mediate the dramatic thermal runaway.

Author Contributions: Conceptualization, H.H.; methodology, J.D. and H.H.; formal analysis, H.H.; investigation, J.D. and H.H.; data curation, J.D. and H.H.; writing—original draft preparation, H.H.; writing—review and editing, H.H.; supervision, H.H. All authors have read and agreed to the published version of the manuscript.

Funding: This research received no external funding.

Conflicts of Interest: The authors declare no conflict of interest.

References

1. Balakrishnan, P.G.; Ramesh, R.; Kumar, T.P. Safety mechanisms in lithium-ion batteries. *J. Power Sources* **2006**, *155*, 401–414. [[CrossRef](#)]
2. Wen, J.; Yu, Y.; Chen, C. A Review on lithium-ion batteries safety issues: Existing problems and possible solutions. *Mater. Express* **2012**, *2*, 197–212. [[CrossRef](#)]
3. Wang, Q.; Ping, P.; Zhao, X.; Chu, G.; Sun, J.; Chen, C. Thermal runaway caused fire and explosion of lithium ion battery. *J. Power Sources* **2012**, *208*, 210–224. [[CrossRef](#)]
4. Feng, X.; Ouyang, M.; Liu, X.; Lu, L.; Xia, Y.; He, X. Thermal runaway mechanism of lithium ion battery for electric vehicles: A review. *Energy Storage Mater.* **2018**, *10*, 246–267. [[CrossRef](#)]
5. Liu, K.; Liu, Y.; Lin, D.; Pei, A.; Cui, Y. Materials for lithium-ion battery safety. *Sci. Adv.* **2018**, *4*, eaas9820. [[CrossRef](#)]
6. Feng, X.; Ren, D.; He, X.; Ouyang, M. Mitigating Thermal Runaway of Lithium-Ion Batteries. *Joule* **2020**, *4*, 743–770. [[CrossRef](#)]
7. Song, L.; Zheng, Y.; Xiao, Z.; Wang, C.; Long, T. Review on Thermal Runaway of Lithium-Ion Batteries for Electric Vehicles. *J. Electron. Mater.* **2022**, *51*, 30–46. [[CrossRef](#)]
8. Goodenough, J.B.; Singh, P. Review—Solid Electrolytes in Rechargeable Electrochemical Cells. *J. Electrochem. Soc.* **2015**, *162*, A2387–A2392. [[CrossRef](#)]
9. Manthiram, A.; Yu, X.; Wang, S. Lithium battery chemistries enabled by solid-state electrolytes. *Nat. Rev. Mater.* **2017**, *2*, 16103. [[CrossRef](#)]
10. Capuano, F.; Croce, F.; Scrosati, B. Composite polymer electrolytes. *J. Electrochem. Soc.* **1991**, *138*, 1918–1922. [[CrossRef](#)]
11. Agrawal, R.C.; Pandey, G.P. Solid polymer electrolytes: Materials designing and all-solid-state battery applications: An review. *J. Phys. D Appl. Phys.* **2008**, *41*, 3715–3725. [[CrossRef](#)]
12. Gao, Z.; Sun, H.; Fu, L. Promises, challenges, and recent progress of inorganic solid-state electrolytes for all-solid-state lithium batteries. *Adv. Mater.* **2018**, *30*, 1705702. [[CrossRef](#)]

13. Chen, L.; Li, Y.; Li, S.; Fan, L.; Nan, C.; Goodenough, J. PEO/garnet composite electrolytes for solid-state lithium batteries: From ‘ceramic-in-polymer’ to ‘polymer-in-ceramic’. *Nano Energy* **2018**, *46*, 176–184. [[CrossRef](#)]
14. Wu, Y.; Wang, S.; Li, H.; Chen, L.; Wu, F. Progress in thermal stability of all-solid-state-Li-ion batteries. *InfoMat* **2021**, *3*, 827–853. [[CrossRef](#)]
15. Masoud, E.M.; El-Bellihi, A.-A.; Bayoumy, W.; Mousa, M. Organic–inorganic composite polymer electrolyte based on PEO–LiClO₄ and nano-Al₂O₃ filler for lithium polymer batteries: Dielectric and transport properties. *J. Alloy. Compd.* **2013**, *575*, 223–228. [[CrossRef](#)]
16. Choi, J.; Lee, C.-H.; Yu, J.-H.; Doh, C.-H.; Lee, S.-M. Enhancement of ionic conductivity of composite membranes for all-solid-state lithium rechargeable batteries incorporating tetragonal Li₇La₃Zr₂O₁₂ into a polyethylene oxide matrix. *J. Power Sources* **2015**, *274*, 458–463. [[CrossRef](#)]
17. Zhao, Y.; Huang, Z.; Chen, S.; Chen, B.; Yang, J.; Zhang, Q.; Ding, F.; Chen, Y.; Xu, X. A promising PEO/LAGP hybrid electrolyte prepared by a simple method for all-solid-state lithium batteries. *Solid State Ion.* **2016**, *295*, 65–71. [[CrossRef](#)]
18. Chen, B.; Huang, Z.; Chen, X.; Zhao, Y.; Xu, Q.; Long, P.; Chen, S.; Xu, X. A new composite solid electrolyte PEO/Li₁₀GeP₂S₁₂/SN for all-solid-state lithium battery. *Electrochim. Acta* **2016**, *210*, 905–914. [[CrossRef](#)]
19. Wang, W.; Yi, E.; Fici, A.J.; Laine, R.M.; Kieffer, J. Lithium ion conducting poly(ethylene oxide)-based solid electrolytes containing active or passive ceramic nanoparticles. *J. Phys. Chem. C* **2017**, *121*, 2563–2573. [[CrossRef](#)]
20. Blake, A.J.; Kohlmeyer, R.R.; Hardin, J.O.; Carmona, E.A.; Maruyama, B.; Berrigan, J.D.; Huang, H.; Durstock, M.F. 3D printable ceramic-polymer electrolytes for flexible high-performance Li-ion batteries with enhanced thermal stability. *Adv. Energy Mater.* **2017**, *7*, 1602920. [[CrossRef](#)]
21. Wang, X.; Zhang, Y.; Zhang, X.; Liu, T.; Lin, Y.; Li, L.; Shen, Y.; Nan, C. Lithium-salt-rich PEO/Li_{0.3}La_{0.557}TiO₃ interpenetrating composite electrolyte with three-dimensional ceramic nano-backbone for all-solid-state lithium-ion batteries. *ACS Appl. Mater. Interfaces* **2018**, *10*, 24791–24798. [[CrossRef](#)] [[PubMed](#)]
22. Zhu, L.; Zhu, P.; Fang, Q.; Jing, M.; Shen, X.; Yang, L. A novel solid PEO/LLTO-nanowires polymer composite electrolyte for solid-state lithium-ion battery. *Electrochim. Acta* **2018**, *292*, 718–726. [[CrossRef](#)]
23. Cha, J.H.; Didwal, P.N.; Kim, J.M.; Chang, D.R.; Park, C.-J. Poly(ethylene oxide)-based composite solid polymer electrolyte containing Li₇La₃Zr₂O₁₂ and poly(ethylene glycol) dimethyl ether. *J. Membr. Sci.* **2019**, *595*, 117538. [[CrossRef](#)]
24. Xia, Y.; Fujieda, T.; Tatsumi, K.; Prosini, P.P.; Sakai, T. Thermal and electrochemical stability of cathode materials in solid polymer electrolyte. *J. Power Sources* **2001**, *92*, 234–243. [[CrossRef](#)]
25. Angulakshmi, N.; Dhanalakshmi, R.B.; Kathiresan, M.; Zhou, Y.; Stephan, A.M. The suppression of lithium dendrites by a triazine-based porous organic polymer-laden PEO-based electrolyte and its application for all-solid-state lithium batteries. *Mater. Chem. Front.* **2020**, *4*, 933–940. [[CrossRef](#)]
26. Joost, M.; Kunz, M.; Jeong, S.; Schonhoff, M.; Winter, M.; Passerini, S. Ionic mobility in ternary polymer electrolytes for lithium-ion batteries. *Electrochim. Acta* **2012**, *86*, 330–338. [[CrossRef](#)]
27. Cheng, S.H.-S.; He, K.-Q.; Liu, Y.; Zha, J.-W.; Kamruzzaman, M.d.; Ma, R.L.-W.; Dang, Z.-M.; Li, R.K.; Chung, C. Electrochemical performance of all-solid-state lithium batteries using inorganic lithium garnets particulate reinforced PEO/LiClO₄ electrolyte. *Electrochim. Acta* **2017**, *253*, 430–438. [[CrossRef](#)]
28. Piana, G.; Bella, F.; Geobaldo, F.; Meligrana, G.; Gerbaldi, C. PEO/LAGP hybrid solid polymer electrolytes for ambient temperature lithium batteries by solvent-free, “one pot” preparation. *J. Energy Storage* **2019**, *26*, 100947. [[CrossRef](#)]
29. Thokchom, J.S.; Gupta, N.; Kumar, B. Superionic Conductivity in a Lithium Aluminum Germanium Phosphate Glass–Ceramic. *J. Electrochem. Soc.* **2008**, *155*, A915–A920. [[CrossRef](#)]
30. Kumar, B.; Kumar, J.; Leese, R.; Fellner, J.P.; Rodrigues, S.J.; Abraham, K.M. A solid state rechargeable long cycle life lithium-air battery. *J. Electrochem. Soc.* **2009**, *157*, A50. [[CrossRef](#)]
31. Chung, H.; Kang, B. Increase in grain boundary ionic conductivity of Li_{1.5}Al_{0.5}Ge_{1.5}(PO₄)₃ by adding excess lithium. *Solid State Ionics* **2014**, *263*, 125–130. [[CrossRef](#)]
32. Robinson, J.P.; Kichambare, P.D.; Deiner, J.L.; Miller, R.; Rottmayer, M.A.; Koenig, G.M., Jr. High temperature electrode-electrolyte interface formation between LiMn_{1.5}Ni_{0.5}O₄ and Li_{1.4}Al_{0.4}Ge_{1.6}(PO₄)₃. *J. Am. Ceram. Soc.* **2018**, *101*, 1087–1094. [[CrossRef](#)]
33. Jung, Y.-C.; Lee, S.-M.; Choi, J.; Jang, S.S.; Kim, D.-W. All Solid-State Lithium Batteries Assembled with Hybrid Solid Electrolytes. *J. Electrochem. Soc.* **2015**, *162*, A704–A710. [[CrossRef](#)]
34. Wang, C.; Yang, Y.; Liu, X.; Zhong, H.; Xu, H.; Xu, Z.; Shao, H.; Ding, F. Suppression of lithium dendrite formation by using LAGP-PEO (LiTFSI) composite solid electrolyte and lithium metal anode modified by PEO (LiTFSI) in all-solid-state lithium batteries. *ACS Appl. Mater. Interfaces* **2017**, *9*, 13694–13702. [[CrossRef](#)]
35. Guo, Q.; Han, Y.; Wang, H.; Xiong, S.; Li, Y.; Liu, S.; Xie, K. New class of LAGP-based solid polymer composite electrolyte for efficient and safe solid-state lithium batteries. *ACS Appl. Mater. Interfaces* **2017**, *9*, 41837–41844. [[CrossRef](#)]
36. Sung, B.-J.; Didwal, P.N.; Verma, R.; Nguyen, A.-G.; Chang, D.R.; Park, C.-J. Composite solid electrolyte comprising poly(propylene carbonate) and Li_{1.5}Al_{0.5}Ge_{1.5}(PO₄)₃ for long-life all-solid-state Li-ion batteries. *Electrochim. Acta* **2021**, *392*, 139007. [[CrossRef](#)]
37. Lee, J.; Howell, T.; Rottmayer, M.; Boeckl, J.; Huang, H. Free-standing LAGP/PEO/LiTFSI composite electrolyte membranes for applications to flexible solid-state lithium-based batteries. *J. Electrochem. Soc.* **2019**, *166*, A416–A422. [[CrossRef](#)]

38. Lee, J.; Rottmayer, M.; Huang, H. Impacts of Lithium Salts on the Thermal and Mechanical Characteristics in the Lithiated PEO/LAGP Composite Electrolytes. *J. Compos. Sci.* **2021**, *6*, 12. [[CrossRef](#)]
39. Sircar, A.K.; Weissman, P.T.; Kumar, B.; Marsh, R. Evaluation of doped polyethylene oxide as solid electrolyte. *Thermochim. Acta* **1993**, *226*, 281–299. [[CrossRef](#)]
40. Lu, Z.; Yang, L.; Guo, Y. Thermal behavior and decomposition kinetics of six electrolyte salts by thermal analysis. *J. Power Sources* **2006**, *156*, 555–559. [[CrossRef](#)]
41. Xuan, X.; Zhang, H.; Wang, J.; Wang†, H. Vibrational Spectroscopic and Density Functional Studies on Ion Solvation and Association of Lithium Tetrafluoroborate in Acetonitrile. *J. Phys. Chem. A* **2004**, *108*, 7513–7521. [[CrossRef](#)]
42. Foran, G.; Mankovsky, D.; Verdier, N.; Lepage, D.; Prébé, A.; Aymé-Perrot, D.; Dollé, M. The Impact of Absorbed Solvent on the Performance of Solid Polymer Electrolytes for Use in Solid-State Lithium Batteries. *iScience* **2020**, *23*, 101597. [[CrossRef](#)] [[PubMed](#)]
43. Commariéu, B.; Paoletta, A.; Collin-Martin, S.; Gagnon, C.; Vijh, A.; Guerfi, A.; Zaghbi, K. Solid-to-liquid transition of polycarbonate solid electrolytes in Li-metal batteries. *J. Power Sources* **2019**, *436*, 226852. [[CrossRef](#)]
44. Chen, P.; Liang, X.; Wang, J.; Zhang, D.; Yang, S.; Wu, W.; Zhang, W.; Fan, X.; Zhang, D. PEO/PVDF-based gel polymer electrolyte by incorporating nano-TiO₂ for electrochromic glass. *J. Sol-Gel Sci. Technol.* **2017**, *81*, 850–858. [[CrossRef](#)]
45. Barroso-Bujans, F.; Fernandez-Alonso, F.; Cerveny, S.; Parker, S.F.; Alegría, A.; Colmenero, J. Polymers under extreme two-dimensional confinement: Poly(ethylene oxide) in graphite oxide. *Soft Matter* **2011**, *7*, 7173–7176. [[CrossRef](#)]
46. Rodrigues, L.; Silva, M.; Veiga, H.; Esperança, M.; Costa, M.; Smith, M.J. Synthesis and electrochemical characterization of aPEO-based polymer electrolytes. *J. Solid State Electrochem.* **2012**, *16*, 1623–1629. [[CrossRef](#)]
47. Zheng, J.; Hu, Y. New insights into the compositional dependence of Li-ion transport in polymer–ceramic composite electrolytes. *ACS Appl. Mater. Interfaces* **2018**, *10*, 4113. [[CrossRef](#)]
48. Enotiadis, A.; Fernandes, N.J.; Becerra, N.A.; Zammarano, M.; Giannelis, E.P. Nanocomposite electrolytes for lithium batteries with reduced flammability. *Electrochim. Acta* **2018**, *269*, 76–82. [[CrossRef](#)]